Heliyon 10 (2024) e39961

Contents lists available at ScienceDirect

Heliyon

journal homepage: www.cell.com/heliyon

Research article

The spatiotemporal and dependency analysis of selected meteorological parameters and normalized difference vegetation index with aerosol optical depth over east Africa

Geoffrey W. Khamala [a,*], John W. Makokha [a], Richard Boiyo [b,c]

[a] Department of Science Technology and Engineering, Kibabii University, P.O. Box 1699-50200, Bungoma, Kenya
[b] Department of Physical Sciences, Meru University of Science and Technology, P.O. Box 972-60200, Meru, Kenya
[c] Department of Environment, Water, Energy and Natural Resources, County Government of Vihiga, Maragoli, Kenya

ARTICLE INFO

Keywords:
Dependency modeling
Spatial and temporal trends
Climatic variables
NDVI

ABSTRACT

The unprecedented rise in atmospheric aerosols, coupled with their intricate interactions with the environment through a wide array of physical, chemical, and biological processes, has profoundly impacted global climate. Their presence in the atmosphere scatters and absorbs solar radiation, thus altering the amount of sunlight reaching the Earth's surface. These direct effects, along with the indirect effects of aerosols, have significantly altered atmospheric temperatures, land surface processes, global surface temperature, hydrological cycle, and ecosystems. Understanding the complex interplay between aerosols and climatic variables necessitates a multidisciplinary approach, such as dependency modeling. Addressing these challenges, the current study conducts a spatiotemporal correlational analysis of selected key meteorological parameters with aerosol optical depth over East Africa (EA) using multisensory data from Moderate-resolution Imaging Spectroradiometer (MODIS), Modern-Era Retrospective analysis for Research and Application (MERRA-2) model, and Tropical Rainfall Measurement Mission (TRMM). Employing a weighted least squares regression (WLS) model, the study quantifies trends in the time series of climatic variables and Normalized Difference Vegetation Index (NDVI), further utilizing a statistical dependency modeling technique for correlational analysis. The trend analysis reveals a significant decreasing trend in surface wind speed (SWS) in most months, with sporadic positive trends attributed to anthropogenic activities, notably biomass burning, observed in January. Spatial trend analysis of Precipitation Rate (PR) displays heterogeneity, with significant negative trends in January and March, and positive trends in February, April, November, and December. Negative trends during May to August are attributed to increased anthropogenic activities, while enhanced positive trends in May correlate with low aerosol optical depth (AOD) during this period. Surface air temperature (SAT) exhibits diverse variations across the region, with dry months recording higher averages and trends than wet months. The study notes heterogeneous correlations in NDVI over the study area, with positive and negative correlations observed in different regions. Specifically, positive correlations are noted along the coastal and Lake Victoria regions, attributed to improved PR enhancing vegetation cover in these areas.

* Corresponding author.
E-mail address: khamalawanjala@gmail.com (G.W. Khamala).

https://doi.org/10.1016/j.heliyon.2024.e39961
Received 18 June 2024; Received in revised form 28 October 2024; Accepted 29 October 2024
Available online 29 October 2024

1. Introduction

The relationships between aerosols and the environment are intricate, involving a multitude of physical, chemical, and biological processes. Their impact on the environment hinges on various factors, including their size, shape, chemical composition, and concentration, as well as the atmospheric conditions they encounter, such as temperature, humidity, and wind speed [1]. Aerosols within the atmosphere scatter and absorb solar radiation, influencing the amount of sunlight reaching the Earth's surface and the atmospheric temperature [2]. Additionally, aerosols serve as cloud condensation nuclei, affecting cloud formation and properties like reflectivity, lifespan, and precipitation rate. Moreover, aerosols can directly and indirectly affect human health and ecosystems. Elevated aerosol concentrations may lead to respiratory and cardiovascular issues in humans, while aerosol deposition may impact soil quality, water quality, and vegetation in ecosystems [3].

Aerosols stand as one of the largest natural systems and catalysts of climate change globally [2,4,5]. They directly influence climate by altering the radiative balance of the Earth-atmosphere system through scattering and absorbing solar and thermal infrared radiations [5–9]. The absorbed radiant energy results in atmospheric warming and surface cooling, impacting atmospheric stability and cloud microphysics, including their lifespan and other characteristics [10]. Furthermore, aerosols indirectly affect land surface processes, global surface air temperature, the climate and hydrological cycle, and ecosystems [11,12].

A comprehensive understanding of the intricate interactions between aerosols and climatic variables within the environment is crucial for predicting and mitigating their impact on climate, air quality, and human health. To achieve this, a multidisciplinary approach encompassing observations, modeling, and experimental studies on the physical, chemical, and biological processes governing aerosol behavior and their environmental impact is necessary across various domains.

EA stands out as a region blessed with abundant natural resources, with agriculture serving as the primary source of sustenance for the majority of its inhabitants. According to the Agriculture Sector Survey of 2023, over 80 % of the workforce is engaged in this sector [13]. However, the region's heavy reliance on rain-fed agriculture, especially in rural and suburban areas, exposes it to significant vulnerability in the face of climate change. Studies indicate a consensus among scientists that rising temperatures and altered precipitation patterns, attributed to climate change, will likely lead to diminished crop yields across many nations [14,15]. Moreover, projections suggest a continual increase in Earth's temperature by 1–3.7 °C by the close of the 21st century [6]. Given these geographical and climatological realities, it is imperative to conduct enhanced correlational analyses between key meteorological factors and atmospheric aerosols in the study region to better align with global development initiatives.

Due to the aforementioned effects, considerable efforts have been directed towards monitoring the spatiotemporal correlation between key climatic variables and aerosols, as well as between climatic variables and vegetation dynamics, particularly the Normalized Difference Vegetation Index (NDVI). These efforts encompass a range of techniques including in situ and ground-based remote sensing measurements, numerical modeling, and satellite-based remote sensing. Analyzing meteorological variables is pivotal in assessing the impacts of climate change and devising necessary adaptation strategies [16]. For example [17], established a relationship between wind speed and aerosol optical depth over Remote Ocean, reporting a high linear correlation within the remote ocean regions with wind speeds ranging from 0 to 20 m/s [18]. identified a positive correlation between AOD and wind speed but suggested caution due to the constant wind speed used in their aerosol retrieval algorithm. Similarly [19], observed an exponential increase in daily averaged AOD with wind speed in Minicoy in the Arabian Sea. Recently [20], examined the relationship between wind speed, temperature, and COVID-19 cases, finding positive correlations between temperature, wind speed, and COVID-19, while relative humidity and air pressure showed inverse correlations. [21], using one-month AOD data from the Sea-viewing Wide Field-of-view Sensor (SeaWiFS) and 10m wind data from ECMWF, identified a power-law relationship between wind speed and AOD for the north Pacific.

The NDVI, derived from near-infrared and red bands of the electromagnetic spectrum, serves as a crucial indicator of vegetation health monitoring, phenology studies, productivity, and crop yield studies across vast areas [22–24]. Numerous studies have explored vegetation responses to specific climatic variables such as precipitation [24–27] and temperature [28–30]. Precipitation and temperature are among the major factors influencing plant photosynthesis, respiration, and growth [31]. Investigated the correlation between NDVI and selected meteorological variables (precipitation, sunshine, air temperature) over Lake Baiyangdian, highlighting a hydro-climatological influence between climatic factors and NDVI.

Despite progress, the current study domain trails the global community in studies related to spatial correlation and trend analysis of climatic variables and vegetation dynamics [8,32]. For instance, studies on the effect of wind on aerosols over EA have predominantly focused on aerosol concentration, size distribution, and the effect of long-range transport [33], indicating a definite correlation between surface wind speed and AOD [8] over EA. However, little is known on the current domain about the influence of surface wind speed on absorption AOD (AAOD) and scattering AOD (SAOD). While similar studies have been conducted in different domains, the current region lags behind in addressing this specific concern. Substantial knowledge on the spatial correlation between aerosol optical properties and key meteorological parameters, as well as between key meteorological parameters and NDVI, which play a crucial role in evaluating climate change [34,35], is largely lacking in EA.

Keeping in mind the aforementioned demand, the present study extends and compliments previous works by investigating spatiotemporal and dependency analysis of selected meteorological parameters with aerosol optical depth over EA. The findings will be of importance to the policymakers in the process of strategizing to combat the forementioned effect on climate change. Detailed material and methods regarding data source and statistical models are described in Section 2 while results and discussion are explained in Section 3. Finally, the executive summary is presented in section. 4.

2. Study area and meteorology

The study was conducted in Eastern Africa (EA), which spans latitudes 12°S to 5°N and longitudes 28°E to 42°E, encompassing Kenya, Uganda, and Tanzania [5]. The region is bordered by Ethiopia and Sudan to the north, Somalia and the Indian Ocean to the east, Rwanda, Burundi, and the Democratic Republic of the Congo (DRC) to the west, and Mozambique and Zambia to the south. EA features a diverse landscape, ranging from glaciated mountains and plateaus to coastal plains, with altitudes varying from sea level to the highest peak at 5895 m (Mount Kilimanjaro) [2,5,33]. The climatological of the study domain has been detailed by previous researchers such as [2,5,8] among others.

2.1. Instrumentation and data

The MODIS sensor, MERRA-2 model and TRMM platforms were used by the current study. MODIS was first launched into the Earth's orbit on 18th, December 1999 onboard the Terra satellite while the second on 4th, May 2002 [36]. The framework captures data in multiple spectral bands, ranging from visible to thermal infrared wavelengths [37–39] and provides global coverage of the Earth's surface every 1–2 days, over 36 spectral bands ranging in wavelengths. Detailed information concerning the sensor, data products, retrieval algorithms, calibration, and uncertainties has been discussed by Refs. [38–42]. The present study utilized Collection 6.1 (C006.1), Level 3 monthly $TAOD_{550}$ retrieved from MODIS Terra at a spatial resolution of $1^\circ \times 1^\circ$ for a period of 18 years (January 2001 to December 2019) to study correlation over EA. While to analyze the NDVI over EA, MOD13Q1 data product (LAADS DAAC) at spatial resolution of 250 m was used.

The MERRA-2 model was launched by the NASA in 2009 [43]. The model is based on GEOS-5 atmospheric data spanning 1980 to present at $0.5^\circ \times 0.625^\circ$ resolution [43–45]. A detailed explanation of MERRA-2 model has been outlined in a previous study by Ref. [5]. The present study, MERRA-2 M2TMNXAER v5.12.4 level-3 monthly time-averaged data for SWS and SAT are retrieved for the analysis of trends in at a spatial resolution of $0.5^\circ \times 0.625^\circ$ from January 2001 to December 2019.

Further, TRMM that is conjointly maintained by NASA and Japan Aerospace Exploration Agency (JAXA) was launched in November 1997 at an altitude of 402.5 km [46]. It was designed to measure rainfall and other precipitation over the tropics and has in itself five instruments that work conjointly i.e., Visible Infrared Scanner (VIRS), Precipitation Radar (PR), Clouds and Earths Radiant Energy System (CERES), TRMM Microwave Imager (TMI) and Lightning Imaging Sensor (LSI) for rainfall suite measurements. The TMI and PR therefore are the main instruments used for precipitation [47] measurements. In current study, TRMM provided TRMM_3A12v7 monthly time averaged map for correlational analysis at a spatial resolution of $0.5^\circ \times 0.5^\circ$ from January 2001 to December 2019. The MODIS, MERRA-2 and TRMM data used in this study can be accessed from http://giovanni.gsfc.nasa.gov/giovanni/

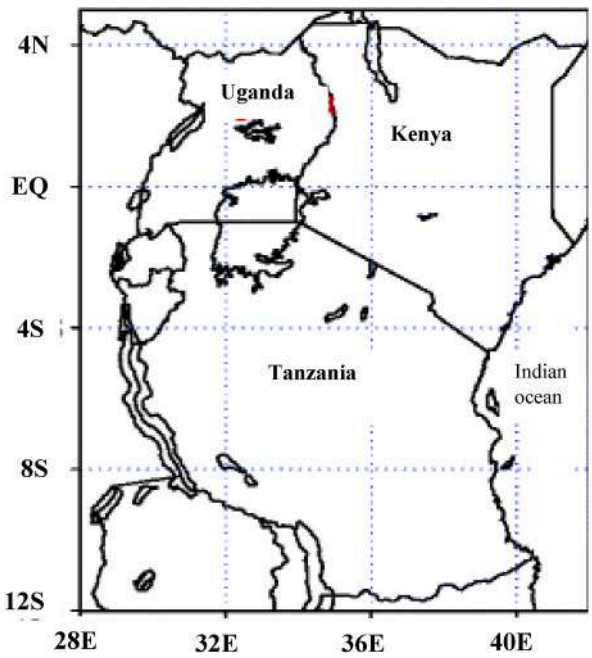

Fig. 1. The study domain showing the main boundaries for Kenya, Uganda and Tanzania. The bounding longitudes and latitudes are shown on the figure.

2.2. Methodology

The overall methodology of this paper is presented in Fig. 2.

2.2.1. Trend analysis

Several approaches have been used to quantify trends in the time series of climatic variable such as nonparametric linear regression and weighted least squares regression (WLS) among other approaches. In the present work, the WLS regression analysis was used to estimate monthly trends in PR, SWS, T and NVDI over EA. The WLS method has been discussed extensively by Ref. [47] and used in many related studies [5,8,46,48–52]. Following this method, a linear trend model (Eq. (1)) was adopted as

$$Y_t = \mu + \omega X_t + N_t, t = 1, 2, \ldots, T \tag{1}$$

where Y_t is the climatic variable for which the trend is being estimated, μ is the offset (y-intercept) which represents the value of Y_t at the beginning of the time series, X_t is the independent variable representing time, ω is the trend estimate of the climatic variable ($n = \frac{T}{12}$), whereas N_t is the residual on the straight line of fit.

2.2.2. Dependency modelling

Dependency modeling is a statistical method used to analyze the relationships between variables and identify the dependencies among them [53]. The study delineated both spatial and linear dependency between NDVI and each climatic variable using Pearson's correlation coefficient (R_{xy}). R_{xy} is calculated between AOD, NDVI and climatic variable using the following equation (2):

$$R_{xy} = \frac{\sum_{i=1}^{n} (y_i - \overline{y})(x_i - \overline{x})}{\sqrt{\sum_{i=1}^{n} (y_i - \overline{y})^2} \sqrt{\sum_{i=1}^{n} (x_i - \overline{x})^2}} \tag{2}$$

where R_{xy} is the Pearson correlation coefficient between variable x and variable y, with a value between −1 and 1, n is the sample size, x_i is the value of NDVI or AOD in the i^{th} month, and y_i is the mean monthly climate variable in the i^{th} month while $\overline{x}$ and $\overline{y}$ are the means of the two variables whose correlation is being calculated.

The NDVI which quantifies the presence and health of vegetation based on remote sensing data was calculated using equation 3

$$NDVI = \frac{NIR - RED}{NIR + RED} \tag{3}$$

Where NDVI was obtained by subtracting the reflectance in the red spectral band from the Near-Infrared (NIR) band [53]. Then, it was divided by the sum of the NIR and red reflectance with the value falling between −1 and +1. The values between −1 and 0 indicate dead plants, or inorganic objects such as stones, roads, and houses whereas the values for live plants range between 0 and 1, with 1 being the healthiest and 0 being the least healthy. The output of this analysis has given an insight in the relationship between the selected climatic parameters, NDVI and the aerosol optical depths over East Africa. This information can be useful for understanding the impact of climatic parameters on aerosol optical depths and vice versa, which can help in developing strategies for mitigating the effects of aerosol pollution in the region.

3. Results and discussion

3.1. Spatial trends in SWS

The SWS (Surface Wind Speed) is a crucial climatic variable that influence the distribution of aerosols in a region by transporting aerosol particles from one place to another [54]. This variable is primarily influenced by two factors: the pressure gradient force and friction. The pressure gradient force is largely generated by temperature differences, with greater temperature disparities leading to stronger winds [55]. On the other hand, friction is caused by obstructions such as tall buildings and vegetation [20].

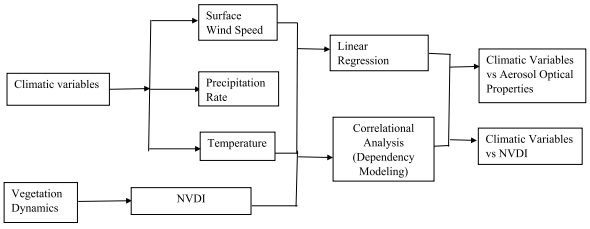

Fig. 2. Overview of the present work.

Fig. 3 illustrates the long-term monthly spatial trend in SWS. Notably, Eastern Africa (EA) shows a significantly decreasing trend in SWS at a 90 % significance level for most months, while some regions exhibit positive trends. These spatial trends indicate continuous changes in SWS due to increased anthropogenic activities. The significantly positive trends observed in March and May (local wet months) suggest an increase in activities such as bush clearing in January and February, which has reduced friction. Additionally, the temperature differences between the niche and surrounding areas could also contribute to increased SWS.

Conversely, negative trends at a 90 % significance level are recorded for most months. These trends can be attributed to rising atmospheric temperatures, which reduce the pressure gradient, and improved environmental conservation laws. The analysis indicates that the negative trends suggest a potential decrease in surface wind-induced aerosol over EA.

3.2. Spatial trends in PR

Fig. 4 illustrates the spatial trends in precipitation (PR) over Eastern Africa (EA) during the study period, with increases and decreases depicted by positive and negative values, respectively. The trends in PR exhibit considerable heterogeneity, being significantly negative in some months (January and March) and significantly positive in others (February, April, November, and December). However, negative trends dominate in May, June, July, and August, likely due to increased anthropogenic activities such as bush clearing and industrialization, which contribute to higher aerosol optical depth (AOD) over the region.

The trends in PR during these months correspond to the patterns observed in total AOD, with negative trends primarily occurring during the local dry months, and low positive trends appearing sporadically [46]. Conversely, the positive trends in PR could be attributed to the implementation of improved environmental conservation laws [46].

3.3. Spatial analysis in SAT

Fig. 5 presents the spatial analysis of Surface Air Temperature (SAT) in Kelvin (K) averaged over the entire study period. The SAT records from 2001 to 2019 for Eastern Africa (EA) show significant monthly, annual, and seasonal variations across the region. The spatial patterns of monthly mean SAT reveal distinct variations, characterized by low, moderate, and high temperatures.

Low SAT values (<289K) are predominantly observed in highly vegetated areas with relatively high altitudes and more rainfall, specifically in the western and central parts of Kenya and the central and southeastern parts of Tanzania. In contrast, moderate to high SAT values (>289K) are found in the arid and semi-arid areas of eastern and northern Kenya and the coastal region. The high SAT in

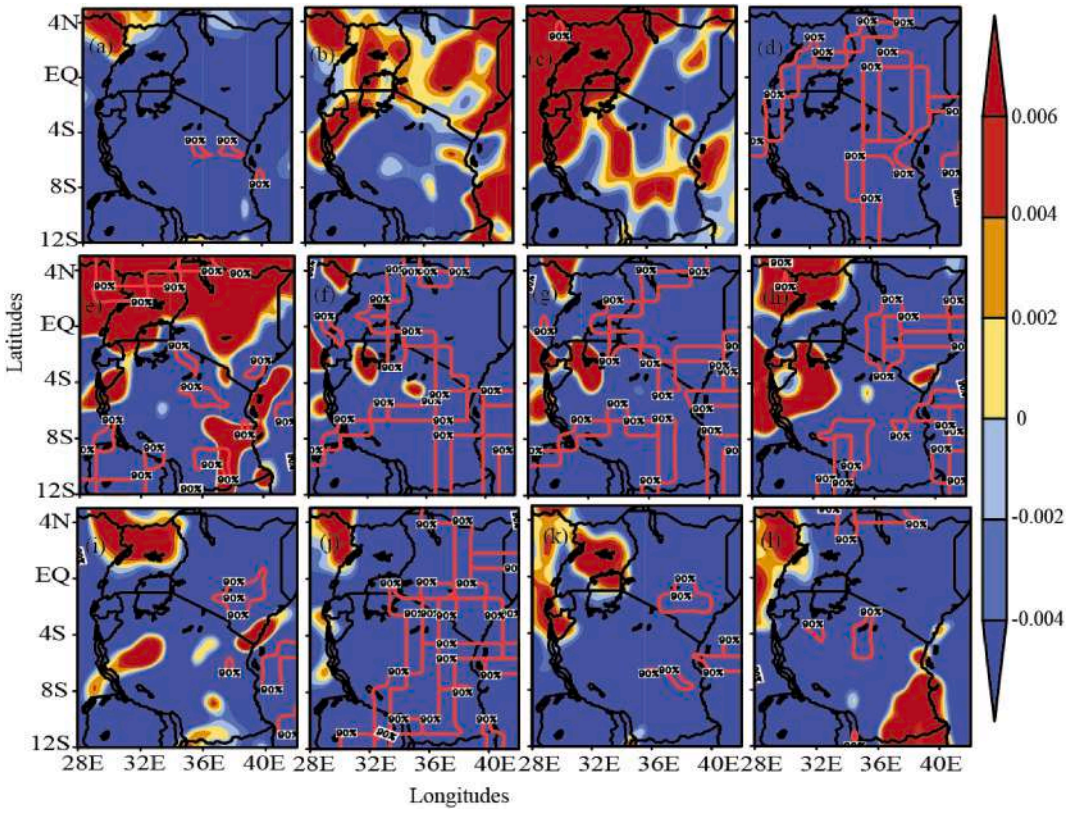

Fig. 3. Spatial trends in surface wind speed over EA, averaged over the entire period of study. The shadings show the sign and magnitude of trend, while the confidence levels are also shown.

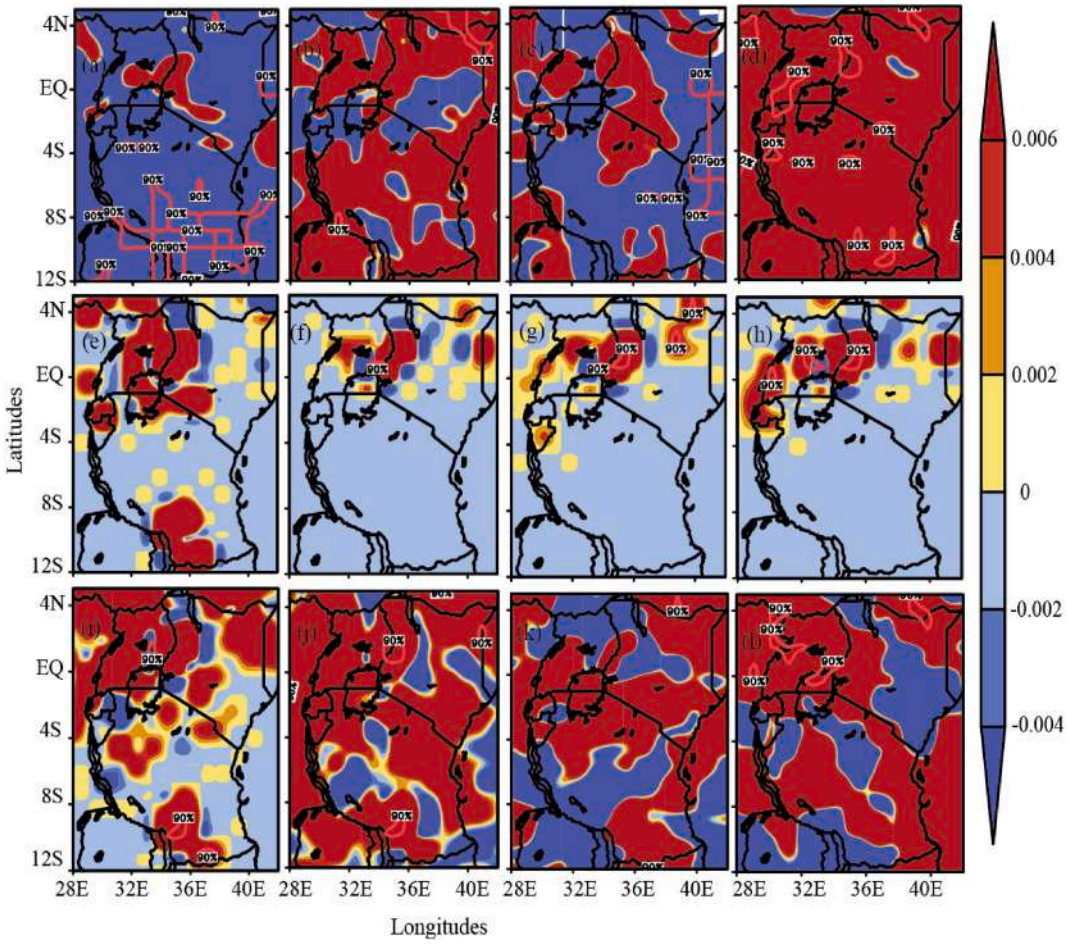

Fig. 4. Spatial trends in precipitation rate over EA, averaged over the entire period of study. The shadings show the sign and magnitude of trend, while the confidence levels are also shown.

these regions could be attributed to increased atmospheric aerosols that absorb heat energy, causing warming in the lower atmosphere [2].

The monthly averages depicted in Fig. 5 have been used to determine the monthly trends in SAT over the study domain, with the results tabulated in Table 1.

3.4. Dependency analysis

Fig. 6 presents the correlations between total aerosol optical depth (TAOD), scattering aerosol optical depth (SAOD), and various meteorological elements, including precipitation (PR) and surface wind speed (SWS). The correlation between TAOD and PR, as well as SAOD and PR, ranges from strong negative to weak positive (Fig. 6a and c, respectively). Notably, there is a significant negative correlation between PR and TAOD, with coefficients greater than 0.6 in some pixels in the northwestern region. This negative correlation is attributed to the unpredictable nature of rainfall, leading to heterogeneous trends in the study area [46]. Increased PR enhances aerosol scavenging, which reduces aerosol loading due to fewer emissions from the wet surface, resulting in lower TAOD and SAOD values. Conversely, during dry periods, aerosol emissions from deserts and biomass burning events increase, and reduced aerosol scavenging through dry deposition fails to remove aerosol particles effectively, leading to higher TAOD and SAOD values.

The spatial correlation between TAOD and SWS, as well as SAOD and SWS, has also been analyzed for the period from 2001 to 2019 (Fig. 6b and d). The correlation coefficient varies from strong positive to strong negative across the entire domain. Results indicate a significant positive correlation between SWS and TAOD, and between SWS and SAOD, with coefficients (r) greater than 0.6 or less than −0.6. As a dynamic force, SWS plays a crucial role in determining TAOD loading over the study area [54]. Local winds, driven by temperature differences between regions, transport aerosols from high-pressure to low-pressure areas, with the magnitude of SWS dependent on the pressure gradient between these regions. Overall, Fig. 6 highlights that TAOD loading in the study domain is most affected by meteorological factors, particularly SWS, PR, and SAT.

The impact of environmental covariates on AOD and its components (AAOD and SAOD) over EA is primarily influenced by the

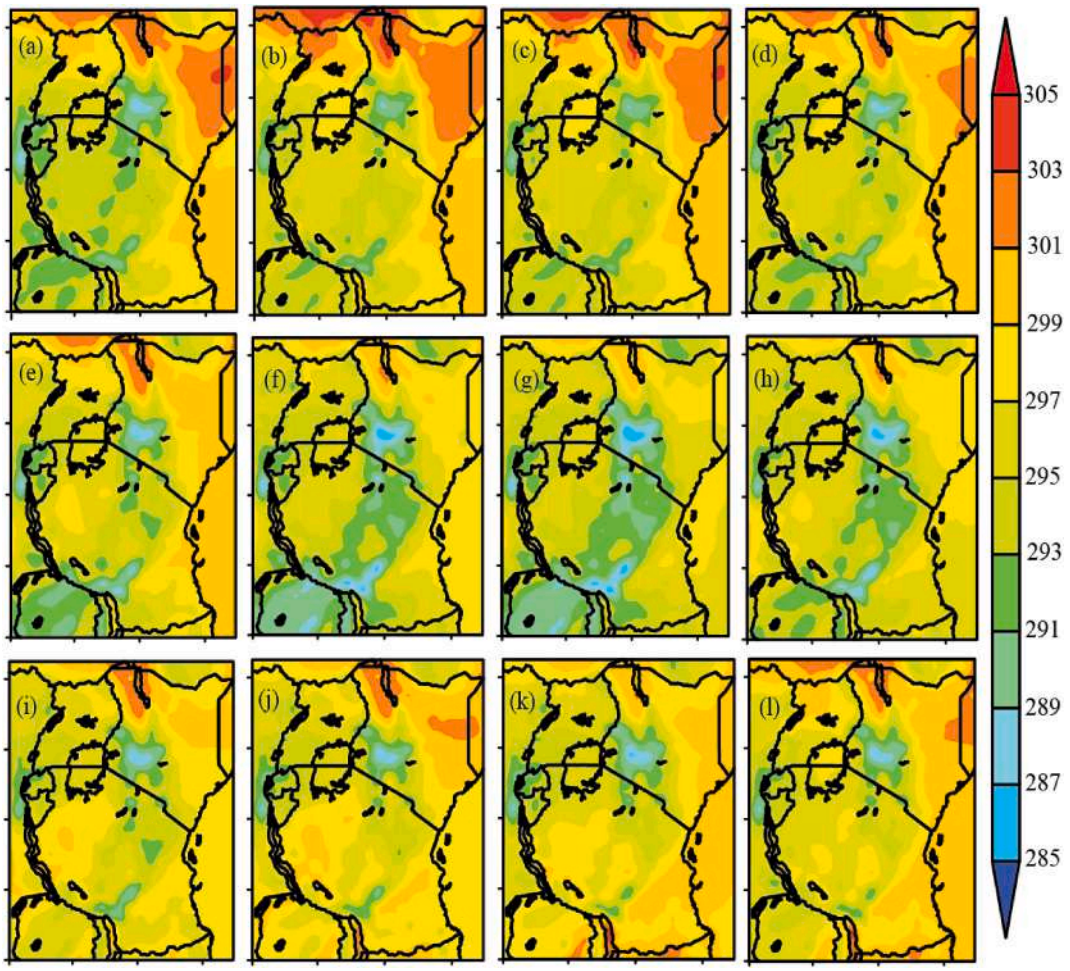

Fig. 5. Spatial analysis in surface air temperature over EA, averaged over the entire period of study. The shadings show the magnitude of surface air temperature over every pixel.

Table 1
The monthly Mean trends in SWS, PR and NDVI over EA.

Month/Variable	SWS	PR	SAT	NDVI
January	−0.012 ± 0.008	0.073 ± 0.039	0.010 ± 0.014	−0.001 ± 0.002
February	−0.0120 ± 0.007	0.001 ± 0.001	0.019 ± 0.014	−0.001 ± 0.001
March	−0.010 ± 0.010	−0.001 ± 0.001	0.004 ± 0.017	0.000 ± 0.001
April	−0.024 ± 0.012	−0.001 ± 0.002	0.011 ± 0.016	−0.000 ± 0.001
May	0.001 ± 0.006	−0.002 ± 0.001	0.037 ± 0.010	0.000 ± 0.001
June	−0.016 ± 0.008	−0.001 ± 0.000	0.029 ± 0.015	0.000 ± 0.001
July	−0.005 ± 0.010	−0.000 ± 0.000	0.033 ± 0.014	0.000 ± 0.001
August	−0.014 ± 0.008	−0.000 ± 0.000	0.017 ± 0.010	0.001 ± 0.001
September	−0.013 ± 0.008	0.000 ± 0.001	0.025 ± 0.010	0.000 ± 0.001
October	−0.022 ± 0.007	0.001 ± 0.001	0.018 ± 0.010	0.001 ± 0.001
November	−0.009 ± 0.011	−0.001 ± 0.002	0.004 ± 0.012	0.000 ± 0.001
December	−0.010 ± 0.013	0.001 ± 0.002	0.010 ± 0.015	−0.000 ± 0.002

Normalized Difference Vegetation Index (NDVI), precipitation rate, surface air temperature, and surface wind speed. The dependency modeling of AOD versus these parameters is analyzed and presented in Fig. 7.

Fig. 7a shows that NDVI correlates heterogeneously with TAOD across the study domain, with both positive and negative correlations observed. NDVI is not a major influencing factor for AOD in the northern part of EA, likely due to the region's distance from the ocean. The cold, humid air currents from the Indian Ocean struggle to reach this desert area, where precipitation is extremely low, sand is frequently blown by the wind, and vegetation struggles to survive [56].

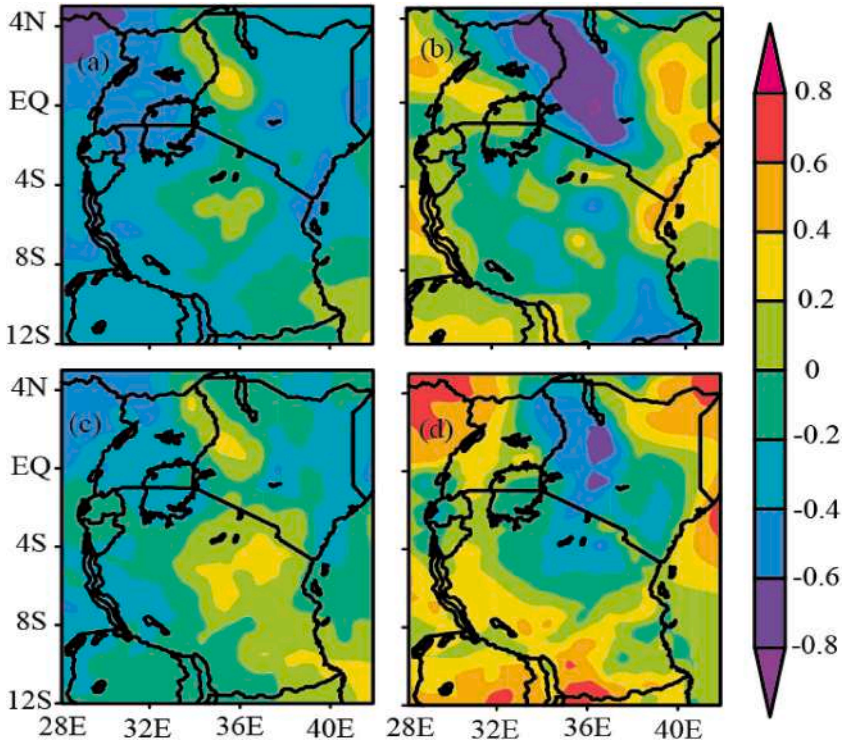

Fig. 6. spatial correlational analysis over EA for (a) TAOD verses PR, (b) TAOD verses SWS, (c) SAOD verses PR and (d) SAOD verses SWS during 2001–2019 period. The shadings show the sign and magnitude of correlation.

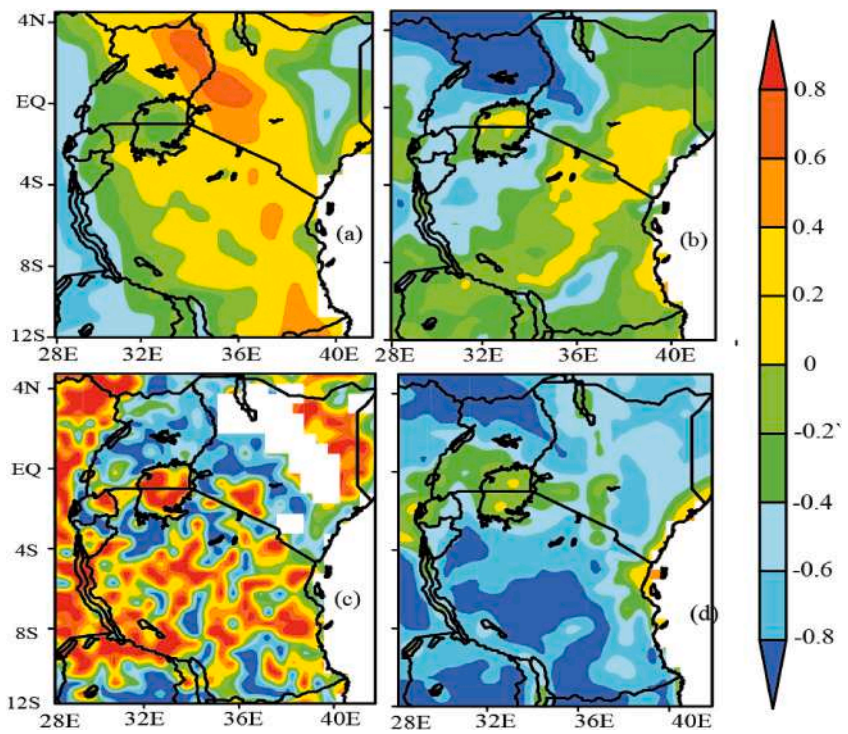

Fig. 7. Spatial correlational analysis over EA. (a) AOD verses NDVI; (b) SAT verses NDVI, (c) PR verses NDVI and (d) SWS verses NDVI. The color bar shows the correlation coefficient (r) over the study domain.

Fig. 7b indicates a negative correlation between NDVI and temperature over most of the study domain, with a positive correlation noted along the coastal region and around Lake Victoria. NDVI responds strongly to changes in rainfall (R~0.75) compared to temperature and elevation. Generally, NDVI values decrease at both very high and very low temperatures.

Fig. 7c shows that NDVI is positively correlated with precipitation over most of the study domain, reinforcing that NDVI responds strongly to changes in rainfall. NDVI values decrease at very high temperatures, as depicted in the northeastern parts of EA [57,58].

Fig. 7d depicts the correlation between NDVI and SWS. Positive correlations are found around large bodies of water, whereas most regions show negative correlations ($r > 0.4$). The positive correlation is attributed to temperature gradients; wind channeling created by large bodies of water, and improved PR around these areas. Near large water bodies, temperature gradients form due to the different thermal properties of land and water. Vegetation thriving on land alters the local microclimate [53,57]. Healthier vegetation (higher NDVI) near water bodies cools the surrounding air through transpiration and shading, potentially influencing wind patterns.

Conversely, the negative correlation depicted in Fig. 7d ($r > 0.8$) is attributed to vegetation density, which offers wind resistance, reducing wind speed. Thick vegetation in high-altitude areas increases surface roughness, providing more resistance to wind flow, thereby reducing surface wind speed. Additionally, dense canopy intercepts and slows down wind near the surface.

3.5. Mean trends in SWS, PR, SAT and NDVI

The monthly mean trends of Surface Wind Speed (SWS), Precipitation (PR), Surface Air Temperature (SAT) and Normalized Difference Vegetation Index (NDVI) as selected climatic variables over EA are assessed and tabulated in Table 1. Trends are estimated by computing the mean of trends for all pixels in Fig. 1.

The mean trend of SWS was found to be negative during most months, primarily influenced by an increase in Direct Aerosol Radiative Forcing (DARF) within the atmosphere. This increase in surface temperature leads to a reduced pressure gradient [2]. In contrast, the mean trend of SWS was positive during January, with a magnitude of 0.0014 yearˆ-1, attributed to increased biomass burning.

The mean trend in PR over the study region was found to be heterogeneously distributed, as indicated in Table 1. PR was generally negative during local dry months, attributed to seasonal cycles of rainfall and anthropogenic activities. Conversely, EA experienced an enhanced positive trend in PR during May (0.0023 yearˆ-1), attributed to low AOD during this month. The positive trends observed during most months were ascribed to increased surface temperature due to DARF within the atmosphere [2].

The trends in SAT during the study period, averaged over EA, showed mostly positive values in most months (Table 1). Generally, the local wet months posted lower trends, while the dry months posted higher trends. This pattern was attributed to increased wet scavenging during wet months, which reduces atmospheric aerosols responsible for absorbing radiation and causing atmospheric heating [2]. However, a specific observation is recorded during May, where the highest trend of 0.037 ± 0.010 is registered despite being a local wet month. This trend could be due to the decreasing PR rate over the region as a result of climate change [14,46].

Table 1 also shows the mean monthly trends in NDVI. The trends are predominantly positive in most months, except during January, February, April, and December. The negative trends in January, February, and December, which are local dry months, could be attributed to sparse or no vegetation cover during these periods, resulting in low reflectance in both the Red and NIR bands [59]. The negative trend in April is attributed to increased clouds and cloud shadows, which can cause negative NDVI values by blocking sunlight and reducing the amount of radiation reaching the Earth's surface, resulting in lower reflectance values, especially in the Red band [60]. On the other hand, positive NDVI trends indicate increased vegetation cover and healthy foliage, contributing to higher reflectance in the NIR spectrum [61].

4. Summary and conclusion

The spatiotemporal correlational analysis of selected meteorological parameters with aerosol optical depth (AOD) and NDVI over East Africa has yielded several key conclusions.

1. The spatial and temporal trends in SWS predominantly show a significantly decreasing trend at a 90 % significance level in most months, with a few regions exhibiting significant positive trends. The trends observed in May suggest increased bush clearing in December, January, and February, leading to reduced vegetation cover. The negative trends in most months are attributed to increasing atmospheric temperatures, which reduce the pressure gradient, along with improved environmental conservation laws. This indicates a potential decrease in surface wind-induced aerosols over EA.
2. The correlations between total aerosol optical depth (TAOD), scattering aerosol optical depth (SAOD), and various meteorological elements (PR and SWS) ranged from strong negative to weak positive. There is a clear negative correlation between PR and TAOD, with a coefficient greater than 0.6 in some pixels in the northwestern region, attributed to the unpredictability of rainfall. The correlations between TAOD and SWS, and SAOD and SWS, varied from strong positive to strong negative due to temperature differences between regions. As a dynamic force in AOD loading, SWS plays a crucial role in determining TAOD loading by transporting aerosols from regions of high pressure to low pressure.
3. The mean SAT showed diverse variations across the region, with dry months recording higher averages and trends than wet months. The high SAT during local dry months is attributed to high atmospheric aerosols that absorb heat energy, causing warming in the lower atmosphere. Generally, the trends were positive, with lower trends during local wet months and higher trends during dry months, due to increased (reduced) wet scavenging.

4. The dependency modeling of NDVI showed heterogeneous correlations with PR and SWS across the study domains, being positive in some regions and negative in others. A positive correlation is specifically noted along the coastal region and within the Lake Victoria region, attributed to temperature gradients, wind channeling created by large bodies of water, and improved PR around these regions, which enhance vegetation cover.

CRediT authorship contribution statement

Geoffrey W. Khamala: Writing – original draft, Validation, Methodology, Formal analysis, Data curation, Conceptualization. **John W. Makokha:** Writing – review & editing, Funding acquisition. **Richard Boiyo:** Writing – review & editing.

Declaration of competing interest

The authors declare the following financial interests/personal relationships which may be considered as potential competing interests:Khamala Geoffrey Wanjala reports statistical analysis was provided by Kibabii University. Reports a relationship with that includes:. Has patent pending to. If there are other authors, they declare that they have no known competing financial interests or personal relationships that could have appeared to influence the work reported in this paper.

References

[1] T. Kocsis, I. Kovacs-Szekely, A. Anda, Homogeneity tests and non-parametric analyses of tendencies in precipitation time series in Keszthely, Western Hungary, Theor. Appl. Climatol. 139 (2020) 849–859, https://doi.org/10.1007/s00704-019-03014-4.

[2] G.W. Khamala, J.W. Makokha, R. Boiyo, K.R. Kumar, Spatiotemporal analysis of absorbing aerosols and radiative forcing over environmentally distinct stations in East Africa during 2001–2018, Sci. Total Environ. 864 (2023) (2023) 161041, https://doi.org/10.1016/j.scitotenv.2022.161041.

[3] R. Mohammed, M. Scholz, Climate variability impact on the spatiotemporal characteristics of drought and aridity in arid and semi-arid regions, Water Resour. Manag. 33 (2019) 5015–5033, https://doi.org/10.1007/s11269-019-02397-3.

[4] R. Boiyo, K.R. Kumar, T.L. Zhao, A 10-year record of aerosol optical properties and radiative forcing over three environmentally distinct AERONET sites in Kenya, East Africa, J. Geophys. Res. Atmos. 124 (2019) 1596–1617.

[5] G.W. Khamala, J.W. Makokha, R. Boiyo, R.K. Kumar, Long-term climatology and spatial trends of absorption, scattering and total aerosol optical depths over East Africa during 2001-2019, Environ. Sci. Pollut. Res. (2022), https://doi.org/10.1007/s11356-022-20022-6.

[6] IPCC, in: T.F. Stocker, D. Qin, G.K. Plattner, M. Tignor, S.K. Allen, J. Boschung, A. Nauels, Y. Xia, V. Bex, P.M. Midgley (Eds.), Climate Change 2013: the Physical Science Basis. Contribution of Working Group-I to the Fifth 4 Assessment Report of the Intergovernmental Panel on Climate Change, vol. 6, Cambridge University Press, Cambridge, United Kingdom And New York, NY, USA, 2013, p. 1535, https://doi.org/10.1017/CBO9781107415324.

[7] IPCC, in: V. Masson-Delmotte, P. Zhai, A. Pirani, S.L. Connors, C. Péan, S. Berger, N. Caud, Y. Chen, L. Goldfarb, M.I. Gomis, M. Huang, K. Leitzell, E. Lonnoy, J. B.R. Matthews, T.K. Maycock, T. Waterfield, O. Yelekçi, R. Yu, B. Zhou (Eds.), Climate Change 2021: the Physical Science Basis. Contribution of Working Group I to the Sixth Assessment Report of the Intergovernmental Panel on Climate Change, Cambridge University Press, Cambridge, United Kingdom and New York, NY, USA, 2021, https://doi.org/10.1017/9781009157896.

[8] R.K. Boiyo, R. Kumar, T. Zhao, Optical, microphysical and radiative properties of aerosols over a tropical rural site in Kenya, East Africa: source identification, modification and aerosol type discrimination, Journal AtmosphericEnvironment 177 (2018) 234–252.

[9] R.K. Boiyo, R. Kumara, T. Zhao, Spatial variations and trends in AOD climatology over East Africa during 2002–2016: a comparative study using three satellite data sets, Int. J. Climatol. (2018), https://doi.org/10.1002/joc.5446.

[10] S.A. Twomey, The influence of pollution on the shortwave albedo of clouds, Journalof the Atmospheric Sciences 34 (1977) 1149–1152, https://doi.org/10.1175/1520-0469(1977)034<1149:TIOPOT>2.0.CO, 2.

[11] R.J. Charlson, S.E. Schwartz, J.M. Hales, D. Cess, J.A. Coakley, J.E. Hansen, D.J. Hofmann, Climate forcing by anthropogenic aerosols, Science 255 (1992) 423–430, https://doi.org/10.1126/science.255.5043.423.

[12] V. Ramanathan, P.J. Crutzen, J.T. Kiehl, D. Rosenfeld, Aerosols, climate, and the hydrological cycle, Science 294 (2001) 2119–2124, https://doi.org/10.1126/science.1064034.

[13] Report on the Agriculture Sector Survey over Kenya, 2023.

[14] B. Ayugi, G. Tan, G.T. Gnitou, M. Ojara, V. Ongoma, Historical evaluations and simulations of precipitation over East Africa from Rossby Centre regional climate model, Atmos. Res. 232 (2020) 104705, https://doi.org/10.1016/j.atmosres.2019.104705.

[15] L.C. Stige, J. Stave, K.S. Chan, L. Ciannelli, N. Pettorelli, M. Glantz, N. Stenseth, et al., The effect of climate variation on agro-pastoral production in Africa, Proc. Natl. Acad. Sci. USA 103 (2006) 3049–3053, https://doi.org/10.1073/pnas.0600057103.

[16] A. Asfaw, B. Simane, A. Hassen, A. Bantider, Variability and time series trend analysis of rainfall and temperature in northcentral Ethiopia: a case study in Woleka sub-basin, Weather Clim Extreme 19 (2018) 29–41, https://doi.org/10.1016/j.wace.2017.12.002.

[17] G.W. Khamala, J.O. Odhiambo, J.W. Makokha, Seasonal variability in aerosol microphysical properties over selected rural, urban and maritime sites in Kenya, Open Access Library Journal 5 (2018) e4821, https://doi.org/10.4236/oalib.1104821.

[18] M.I. Mishchenko, I.V. Geogdzhayev, W.B. Rossow, B. Cairns, A.A. Lacis, Global two-channels AVHRR retrievals of aerosol properties over oceans for the period of NOAA-9 observations and preliminary retrievals using NOAA-7 and NOAA-11 data, J. Atmos. Sci. 59 (2007) 262–278.

[19] K.K. Moorthy, S.K. Satheesh, Characteristics of aerosols over a remote island, Minicoy in the Arabian Sea: optical properties and retrieved size characteristics, Q. J. Roy. Meteorol. Soc. 126 (2000) 81–109, 2000.

[20] M. Abdullrahman, On the Relationship between Meteorological Variables, Dust Index, Solar Wind Speed, Solar Radio Flux, and Cosmic Rays and COVID-19 Cases, 2022.

[21] P. Glantz, E.N. Nilsson, W. Hoyningen-Huene, Estimating a relationship between aerosol optical thickness and surface wind speed over the ocean, Atmos. Res. 92 (2009) 58–68.

[22] A.K. Prasad, R.P. Singh, M. Kafatos, A. Singh, Effect of the growing population on the air pollution, climatic variability and hydrological regime of the Ganga Basin, India, in: Proceedings of the Symposium S6 Held during the Seventh IAHS Scientific Assembly, Foz Do Iguacu, Brazil, 3–9 April 2005, IAHS Publication: Foz do Iguacu, Brazil, 2007, p. 295.

[23] I. Rashid, et al., Projected climate change impacts on vegetation distribution over Kashmir Himalayas, Climatic Change 132 (2015) 601–613.

[24] J. Revadekar, Y.K. Tiwari, K.R. Kumar, Impact of climate variability on NDVI over the Indian region during 1981–2010, Int. J. Rem. Sens. 33 (2012) 7132–7150.

[25] N. Dubois, et al., Indonesian vegetation response to changes in rainfall seasonality over the past 25, 000 years Nature Geoscience 7 (2014) 513.

[26] Y.H. Fu, et al., Unexpected role of winter precipitation in determining heat requirement for spring vegetation green-up at northern middle and high latitudes, Global Change Biol. 20 (2014) 3743–3755.

[27] M. Shen, S. Piao, N. Cong, G. Zhang, I.A. Jassens, Precipitation impacts on vegetation spring phenology on the T ibetan P lateau, Global Change Biol. 21 (2015) 3647–3656.

[28] R.B. Myneni, C. Keeling, C.J. Tucker, G. Asrar, R.R. Nemani, Increased plant growth in the northern high latitudes from 1981 to 1991, Nature 386 (1997) 698.

[29] S. Peng, et al., Asymmetric effects of daytime and night-time warming on Northern Hemisphere vegetation, Nature 501 (2013) 88.
[30] S. Piao, et al., Net carbon dioxide losses of northern ecosystems in response to autumn warming, Nature 451 (2008) 49.
[31] F. Wang, X. Wang, Y. Zhao, Z. Yang, Temporal variations of NDVI and correlations between NDVI and hydro-climatological variables at Lake Baiyangdian, China, Int. J. Biometeorol. 58 (2014) 1531–1543.
[32] J.W. Makokha, J.O. Odhiambo, J.G. Shem, Long term assessment of aerosol radiative forcing over selected sites of East Africa, J Geosci Environ Prot\6 (2018) 22–34, https://doi.org/10.4236/gep.2018.64002.
[33] J. Ngaina, J. Muthama, Monitoring spatial-temporal variability of aerosol over Kenya, Ethiop J Environ Stud Manage 7 (2014) 244–252, https://doi.org/10.4314/ejesm.v7i3.2.
[34] A.J. Adesina, S. Piketh, K.R. Kumar, S. Venkataraman, Characteristics of columnar aerosol optical and microphysical properties retrieved from the sun photometer and its impact on radiative forcing over Skukuza (South Africa) during 1999–2010, Environ. Sci. Pollut. Res. 24 (2017) 16160–16171, https://doi.org/10.1007/s11356-017-9211-2.
[35] M. Alam, C. Siwar, B. Talib, M. Mokhtar, M.E. Toriman, Climate change adaptation policy in Malaysia: issues for agricultural sector, Afr. J. Agric. Res. 7 (9) (2012) 1368–1373, https://doi.org/10.5897/AJARX11.030.
[36] L.A. Remer, Y.J. Kaufman, D. Tanre, S. Matto, D.A. Chu, J.V. Martins, et al., The MODIS aerosol algorithm, products, and validation, J Atmos Sci 62 (4) (2005) 947–973, https://doi.org/10.1175/JAS3385.1.
[37] N.C. Hsu, S.C. Tsay, M.D. King, J.R. Herman, Aerosol properties over bright-reflecting source regions, IEEE Trans Geosci Remote Sens 42 (2004) 557–569.
[38] A.M. Sayer, N.C. Hsu, C. Bettenhausen, M.J. Jeong, Validation and uncertainty estimates for MODIS collection 6B Deep Blue aerosol data, J Geophys Res Atmos 118 (14) (2013) 7864–7872, https://doi.org/10.1002/jgrd.50600.
[39] A.M. Sayer, L.A. Munchak, N.C. Hsu, R.C. Levy, C. Bettenhausen, M.J. Jeong, MODIS Collection 6 aerosol products: comparison between aqua's Deep Blue, dark target, and B merged data sets, and usage recommendations, J Geophys Res Atmos 119 (24) (2014) 13965–13989, https://doi.org/10.1002/2014JD022453.
[40] R.C. Levy, L.A. Remer, R.G. Kleidman, S. Mattoo, C. Ichoku, R. Kahn, T.F. Eck, Global evaluation of the collection 5MODIS dark-target aerosol products over land, Atmos Chem Phys 10 (21) (2010) 10399–10420, https://doi.org/10.5194/acp-10-10399-2010.
[41] N.C. Hsu, M.J. Jeong, C. Bettenhausen, A.M. Sayer, R. Hansell, C.S. Seftor, J. Huang, S.C. Tsay, Enhanced Deep Blue aerosol retrieval algorithm: the second generation, J Geophys Res Atmos 118 (16) (2013) 9296–9315, https://doi.org/10.1002/jgrd.50712.
[42] D. Xiao, Y. Li, S.J. Fan, R.H. Zhang, J.H. Sun, Y. Wang, Plausible influence of Atlantic Ocean SST anomalies on winter haze in China, Theor. Appl. Climatol. 122 (2016) 249–257, https://doi.org/10.1007/s00704-014-1297-6.
[43] M.M. Rienecker, J.M. Suarez, R. Gelaro, R. Todling, J. Bacmeister, E. Liu, G.M. Bosilovich, D.S. Schubert, L. Takacs, G. Kim, S. Bloom, J. Chen, D. Collins, A. Conaty, A. Dasilva, W. Gu, J. Joiner, R.D. Koster, R. Lucchesi, et al., MERRA: NASA's modern-era retrospective analysis for research and applications, J Clim 24 (2011), https://doi.org/10.1175/JCLI-D-11-00015.1.
[44] W.S. Wu, R.J. Purser, D.F. Parrish, Three-dimensional variational analysis with spatially inhomogeneous covariances, Mon Weather Rev 130 (2002) 2905–2916.
[45] R. Khan, K.R. Kumar, T. Zhao, W. Ullah, G. de Leeuw, Interdecadal changes in aerosol optical depth over Pakistan based on the MERRA-2 reanalysis data during 1980–2018, Remote Sens 13 (2021) 822, https://doi.org/10.3390/rs13040822.
[46] J. Makokha, J. Odhiambo, J. Godfrey, Trend analysis of aerosol optical depth and Angstrom exponent anomaly over East Africa, Atmos Clim Sci 7 (2017) 588–603, https://doi.org/10.4236/acs.2017.74043.
[47] E.C. Weatherhead, G.C. Reinsel, G.C. Tiao, X.L. Meng, D. Choi, W.K. Cheang, T. Keller, J. DeLuisi, D.J. Wuebbles, J.B. Kerr, A.J. Miller, S.J. Oltmans, J. E. Frederick, Factors affecting the detection of trends: statistical considerations and applications to environmental data, J Geophys Res 103 (D14) (1998) 17149–17161, https://doi.org/10.1029/98JD00995.
[48] K.R. Kumar, V. Sivakumar, Y. Yin, R.R. Reddy, N. Kang, Y. Diao, A.J. Adesina, X. Yu, Long-term (2003–2013) climatological trends and variations in aerosol optical parameters retrieved from MODIS over three stations in South Africa, Atmos Environ 95 (2014) 400–408, https://doi.org/10.1016/j.atmosenv.2014.07.001.
[49] K.R. Kumar, Y. Yin, V. Sivakumar, N. Kang, X. Yu, Y. Diao, A.J. Adesina, R.R. Reddy, Aerosol climatology and discrimination of aerosol types retrieved from MODIS, MISR and OMI over Durban (29.88° S, 31.02° E), South Africa, Atmos Environ 117 (2015) 9–18, https://doi.org/10.1016/j.atmosenv.2015.06.058.
[50] N. Kang, K.R. Kumar, K. Hu, X. Yu, Y. Yin, Long-term (2002–2014) evolution and trend in collection 5.1 level-2 aerosol products derived from the MODIS and MISR sensors over the Chinese Yangtze River Delta, Atmos Res 181 (2016) 29–43, https://doi.org/10.1016/j.atmosres.2016.06.008.
[51] A.J. Adesina, K.R. Kumar, V. Sivakumar, S.J. Piketh, Inter-comparison and assessment of long-term (2004–2013) multiple satellite aerosol products over two contrasting sites in South Africa, J Atmos Sol Terr Phys 148 (2016) 82–95, https://doi.org/10.1016/j.jastp.2016.09.001.
[52] P. Dahutia, B. Pathak, P.K. Bhuyan, Aerosol's characteristics, trends and their climatic implications over Northeast India and adjoining South Asia, Int J Climatol (2017), https://doi.org/10.1002/joc.5240.
[53] G.M. Ghebrezgabher, T. Yang, X. Yang, T.E. Sereke, Assessment of NDVI variations in responses to climate change in the Horn of Africa, The Egyptian Journal of Remote Sensing and Space Sciences 23 (2020) (2020) 249–261.
[54] S.S. Prijith, P. Rao, M. Mohan, M. Sai, M. Ramana, Trends of absorption, scattering and total aerosol optical depths over India and surrounding oceanic regions from satellite observations: role of local production, transport and atmospheric dynamics, Environ. Sci. Pollut. Res. Int. 25 (5) (2017) 1–14, https://doi.org/10.1007/s11356-018-2032-0.
[55] H. Huang, G.E. Thomas, R.G. Grainger, Relationship between wind speed and aerosol optical depth over Remote Ocean, Atmos. Chem. Phys. 10 (2010) 5943–5950, https://doi.org/10.5194/acp-10-5943-2010.
[56] J. Li, X. Ge, Q. He, A. Abbas, Aerosol optical depth (AOD): spatial and temporal variations and association with meteorological covariates in Taklimakan desert, China, The open access journal for life and environmental research (2021), https://doi.org/10.7717/peerj.10542.
[57] F. Hao, X. Zhang, W. Ouyang, A.K. Skidmore, A.G. Toxopeus, Vegetation NDVI linked to temperature and precipitation in the upper catchments of yellow river, Environ. Model Assess 17 (2012) 389–398, https://doi.org/10.1007/s10666-011-9297-8.
[58] H. Yin, T. Udelhoven, R. Fensholt, D. Pflugmacher, P. Hostert, How normalized difference vegetation index (NDVI) trends from advanced very high-resolution radiometer (AVHRR) and Système Probatoired' observation dela Terre VEGETATION (SPOT VGT) time series differ in agricultural areas: an inner Mongolian case study. Rem, Sens. 4 (2012) 3364–3389, https://doi.org/10.3390/rs4113364.
[59] P.S. Thenkabail, J.G. Lyon, A. Huete, A review of remote sensing of vegetation water content: drought monitoring and beyond, in: Proceedings of the IGARSS 2000, IEEE International Geoscience and Remote Sensing Symposium, 2000. http://doi:10.1109/IGARSS.2000.861710.
[60] C.O. Justice, J.R.G. Townshend, B.N. Holben, Analysis of the phenology of global vegetation using meteorological satellite data, International Journal of Remote Sensing 6 (8) (1985) 1271–1318. http://doi:10.1080/01431168508948283.
[61] N. Pettorelli, J.O. Vik, A. Mysterud, J.M. Gaillard, C.J. Tucker, N.C. Stenseth, NDVI derived phenological metrics to detect changes in vegetation phenology, Remote Sensing of Environment 93 (3) (2005) 463–474. http://doi:10.1016/j.rse.2004.08.006.